Bull Volcanol (2006) 68: 349–362
DOI 10.1007/s00445-005-0011-z

RESEARCH ARTICLE

M. Favalli · M. T. Pareschi · G. Zanchetta

Simulation of syn-eruptive floods in the circumvesuvian plain (southern Italy)

Received: 29 April 2003 / Accepted: 20 June 2005 / Published online: 3 November 2005

Abstract During explosive eruptions the deposition of fine-grained volcanic ash fallout reduces soil permeability, favouring runoff of meteoric water and thus increasing the occurrence of catastrophic floods. A fully dynamic, two-dimensional model was used to simulate flooding scenarios in the Vesuvian area following an explosive volcanic eruption. The highest risk occurs in the catchment area of the Acerra-Nola Plain N and NE of Vesuvius. This plain has a population of 70,000 living in low-lying areas. This catchment area is vulnerable to ash fall because it lies downwind of the dominant synoptic circulation and it lacks a natural outflow toward the sea. Our numerical simulations predict dangerous scenarios, even in quiescent periods, during extreme rain events (return periods of 200 years have been considered), and a significant increase in the extent of the flooded areas due to renewed volcanic activity. Based on these simulations a hazard zonation has been proposed.

Keywords Vesuvius · Flood · Flood simulation · Volcanic hazard · Southern Italy · Phreatomagmatic ash · Explosive eruption

Introduction

During, or shortly after, an explosive eruption, heavy or prolonged rainfall can trigger hazardous sediment-laden flows into channels that drain the slopes of the volcano. Meteoric precipitation, through surface runoff that entrains loose pyroclastic material, can trigger debris flows (containing 60–80% vol. of sediment), hyperconcentrated flows (20–60% vol. of sediment) or stream flooding (less than 20% in vol. of sediment). High sediment laden-flows are often called lahars when they initiate on the volcanic slope.

Overland flow and flooding are usually promoted by the "waterproof" effect produced by the deposition of fine volcanic ash layers. Volcanic ash layers are characterised by low hydraulic conductivity which decreases water infiltration in the soils (e.g. McKee et al. 1985; Rosi et al. 1993; Rosi 1996; Shimokawa and Jitousono 1997). It is well known that deposition of volcanic ashes can reduce soil permeability by 10 or 100 times (Shimokawa and Jitousono 1997 and references therein). Explosive volcanic activity resulting from the interaction of rising magma with superficial or deep aquifers is often characterised by enhanced fragmentation of the magma with the generation and deposition, even in proximal areas, of large quantities of fine ash. The role in flood triggering played by cm-to-dm thick blankets of fine-grained ashes of phreatomagmatic origin was demonstrated, for instance, by the 1937 Rabaul (McKee et al. 1985) and A.D. 1631 Vesuvius (Rosi et al. 1993) eruptions. Along with a decrease in soil infiltration, flooding is also provoked by the destruction of vegetation cover that occurs during eruptions.

The dynamic of the eruptive column can also produce atmospheric disturbances, which along with the condensation of water steam of the eruptive cloud may produce anomalous heavy rains. Strictly speaking, the rains that occur during an eruption are those that trigger syn-eruptive lahars and flooding over large areas around a volcano. However, the period of flooding hazard may outlast the eruption by years or even decades (e.g. Newhall and Punongbayan 1996; Major et al. 2000), depending on the climatic regime and the time needed to restore the original soil condition and vegetation cover.

Although the waterproof effect is marked on the volcanic slope, it can be significant downwind along the dispersal axis of fallout ash, so that catchment areas far from the

Editorial responsibility: A. Woods

M. Favalli · M. T. Pareschi (✉)
Istituto Nazionale di Geofisica e Vulcanologia, Via della Faggiola 32,
56126 Pisa, Italy
e-mail: pareschi@pi.ingv.it

G. Zanchetta
Dipartimento di Scienze della Terra, University of Pisa, via S. Maria,
56126 Pisa, Italy

volcano can contribute significantly to the source of catastrophic flooding.

The case history of Vesuvius

Although Vesuvius (southern Italy; Fig. 1) has been dormant since 1944 when the last eruption occurred (Santacroce 1987), it must still be considered a very dangerous active volcano (e.g. Barberi et al. 1990; Luongo et al. 1996; Lirer et al. 1997; Pareschi 2002). During its life, this volcano has experienced long rest periods followed by catastrophic Plinian eruptions or phases characterised by quiet lava emission and moderate to violent Strombolian activity (e.g. Bertagnini et al. 1998; Santacroce 1987; Cioni et al. 2003; Andronico and Cioni 2002; Rolandi et al. 1993a, b, c; Arrighi et al. 2001). The risk in the case of renewed volcanic activity is very high due to the density of human settlements in the surrounding areas (700,000 people live on its slopes and at the foot of the volcano, e.g. Barberi et al. 1990; Pareschi et al. 2000a, b; Pareschi 2002). Even though a great deal of research has been done on different aspects of volcanic risk at Vesuvius (Barberi et al. 1990; Lirer et al. 1997; Pareschi 2002; Cioni et al. 2003; Todesco et al. 2002; among others), so far little attention has been paid to the aspects of flooding (Rosi et al. 1993; Pareschi et al. 2000b; Andronico and Cioni 2002).

At Vesuvius, floods are strictly related to the deposition on the ground of fine-grained low-permeable ash ejected in phreatomagmatic eruptions. Phreatomagmatic activity is quite frequent at Somma-Vesuvius (e.g. Cioni et al. 1992; Rolandi et al. 1993c; Rosi et al. 1993; Santacroce et al. 1993; Sigursson et al. 1985; Andronico and Cioni 2002). Magma-water interaction can occur at two different levels within the volcanic edifice: a shallow level and a deep level. The shallow interaction can occur between the rising magma and small aquifers located inside the volcanic pile of Vesuvius. Generally, this characterises the final stages of low-energy explosive eruptions (i.e. the 1906 event; Santacroce et al. 1993) or the opening phases of large Plinian events (i.e. the Avellino eruption, 3.8 ka; Rolandi et al. 1993c). Deep interaction is also possible, leading to phreatomagmatic eruptions and involving deep magma and phreatic water stocked in the Mesozoic carbonates of the Somma-Vesuvius basement.

Whatever the water source, magma–water interaction may lead to the ejection and deposition of fine, low-permeable, ash deposits as far as tens of km away from the volcanic vent. Related floods occur in a wide area around the volcano, and mainly in the alluvial plain to the N and NE (Acerra-Nola basin), which has no natural drainage towards the sea, this being inhibited by the volcano itself. The catchment areas of these floods are partly on the Somma-Vesuvius slopes, but also, to a greater extent, on the Apennine chain (Fig. 1), E and NE of the volcano.

Syn-eruptive sediment-laden flow and flooding are evidenced geologically by coarse debris flows and fine overbank deposits in considerable numbers of sections both in proximal and distal areas with respect to the volcano (e.g. Pareschi et al. 2002). These deposits rest typically in stratigraphic succession with the primary volcanic deposit, a feature lacking in the inter-eruptive "normal" floods and debris flows (e.g. Zanchetta et al. 2004). Detailed analyses on the recurrence of these deposits are not yet available. Field data are also supported by historical accounts over the last 400 years of the volcano's activity (Cerbai and Principe 1996; Nazzaro 1997). Extensive floods, originating both from the volcanic flanks and Apennine drainage networks,

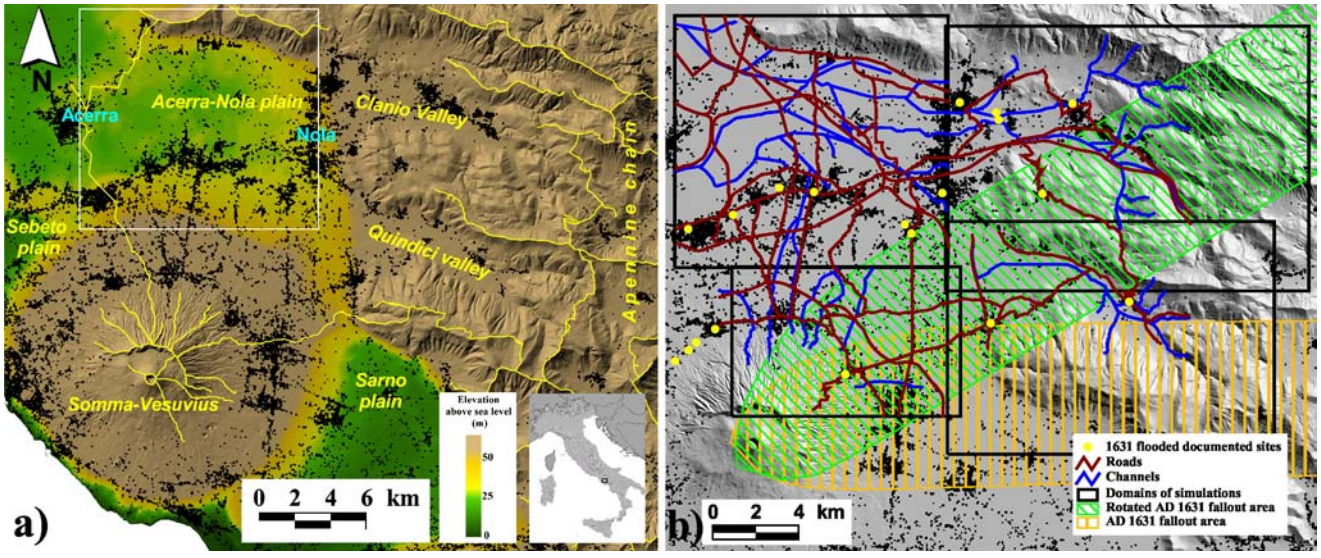

Fig. 1 Map of the study area. **a**) General view of the morphology of Somma-Vesuvius and the surrounding alluvional plains. The *thin yellow lines* correspond to the main watershed. **b**) Domains of the simulations and the road and channel network considered in the simulations. The areas considered waterproofed by the volcanic ash in the simulation are also shown. *Yellow stripes*: ash dispersion within the 10 cm isopach of the A.D. 1631 eruption (after Rosi et al. 1993); *Green stripes*: ash dispersion within the 10 cm isopach, like A.D. 1631, but rotated northwards

occurred in concomitance with the last large Vesuvian eruption of A.D. 1631 on the plain N and NE of the volcano (Acerra-Nola Plain, Fig. 1), causing the inundation and destruction of a number of settlements (Rosi et al. 1993, 1996, Fig. 1). Flooding also took place during the smaller eruptions of A.D. 1794, 1822 and 1906 (Nazzaro 1997). In this regard, a historical chronicle states: "The waters descended from the mountains like streams and their abundance was so high that all people believed a new spring had opened. . .and these (waters) inundated all the plain up to Nola, Merigliano and Cerra . . ." (Ascanio 1632, quoted by Nazzaro 1997), or again: "lots of farmhouses were dragged away by the violence of the torrents, and casualties were not lacking. . ." (Alfano 1906, quoted by Nazzaro, 1997).

The low permeability of the phreatomagmatic deposit is reduced even further if the ashes are dry. An eye-witness account describes in detail this waterproof effect for the 1822 eruption: ". . .the soil was covered by a sort of plaster originating from the fine sand (volcanic ash) and the meteoric rain. They (the people) hurried, therefore, to break at the foot of the mountain the hardened crust and such operations were ordered in all the villages . . ..The communities of Ottaviano, Bosco and Resina, which were more prompt than the others, were saved from the subsequent floods. . ." (quoted in Nazzaro 1997).

A coherent sequence of events emerges from these historical chronicles: fine-grained ashes fell and were hardened by the effect of early rains. The water-resistant hard crusts enhanced surface run-off and decreased infiltration of the subsequent meteoric water into the soil, thus increasing runoff yield and promoting flooding. The historical accounts set important constraints on the rheology of the fluid that inundated the alluvial plains. Indeed, they suggest that the inundations in the Acerra-Nola Plain were primarily low-sediment concentrated flows. This flooding was often described as formed by muddy water, streams or torrents, as opposed to debris flows, which are generally described as mud flows (Principe, 2002, personal communication).

Obviously syn-eruptive and inter-eruptive debris flows may also occur, triggered mainly by the saturation of permeable volcanic deposits and erosion effects. In this case, large amounts of loose volcaniclastic material are quickly mobilised on the volcanic slopes as well as in the Apennine chain, generating high-concentrated flows. However, geological evidence suggests that they remain confined for the most part to the volcanic apron or the alluvial fans at the foot of the Apennine chain (Pareschi et al. 2000b; Pareschi et al. 2002; Migale and Milone 1998; Rosi et al. 1993). The moderate mobility of these debris flow events (compared with that of floods) is also confirmed by the recent case history of Sarno-Quindici: in May of 1998, after intense rainfall, dozens of volcaniclastic debris flows originated at the expense of the volcaniclastic colluvial cover of the hillslopes and stopped at the foot of the slopes (Calcaterra et al. 1999, 2000; Pareschi et al. 2000c; Zanchetta et al. 2004).

In this paper, the flood hazard at Vesuvius is considered. With the aim of dealing with the flood problem quantitatively, a fully dynamic two-dimensional model (O'Brien et al. 1993) was used to simulate different scenarios in the case of a renewal of volcanic activity. The simulations include the floodable area, the flow depth and velocity, from which it was possible to calculate the maximum theoretical pressure exerted by the flow. From the performed simulation a proposal for hazard zonation is also discussed.

Recent works on the calibration and validation of two-dimensional models of river flood inundation (e.g. O'Brein 1999; Bates and De Roo 2000; Horritt and Bates 2001, 2002) have demonstrated that both raster-based and finite-element approaches are useful in reproducing the extent of inundations and the bulk hydrometric responses of river reaches. A two-dimensional approach is indeed capable of resolving some hydraulic processes induced by floodplain topography that a one-dimensional model is unable to do (Horritt and Bates 2001).

The model

The physical process model used in simulations routes rainfall-runoff and flood hydrographs over unconfined surfaces with topographic data files exported from a digitized base map (O'Brien et al. 1993). Flood routing in two dimensions is accomplished through a numerical integration of the equations of motion and the conservation of fluid volume. The constitutive equations include the continuity equation:

$$\partial \mathrm{h}/\partial \mathrm{t} + \partial \mathrm{hV_x}/\partial \mathrm{x} + \partial \mathrm{hV_y}/\partial \mathrm{y} = \mathrm{i} \tag{1}$$

and the two-dimensional equations of motion (dynamic wave equation):

$$S_{\mathrm{fx}} = S_{\mathrm{ox}} - \partial h/\partial x - V_x \partial V_x/g\partial y - V_y \partial V_x/g\partial y - \partial V_x/g\partial t \tag{2}$$

$$S_{fy} = S_{oy} - \partial h/\partial y - V_y \partial V_y/g\partial y - V_x \partial V_y/g\partial x - \partial V_y/g\partial t \tag{3}$$

where h is the flow depth, V_x and V_y are the depth-averaged velocity components along the x- and y-coordinates, and i is the excess rainfall intensity. The equations take into account the pressure gradient, convective and local acceleration terms. S_{fx} and S_{fy} are the friction slope components and S_{ox} and S_{oy} the bed slope. Under the simplified assumption of no erosion and no sediment transport, the energy dissipation term is dealt with via Manning's formula. The differential form of the continuity and momentum equations is solved with a central, finite difference numerical integration method. The numerical schemes are explicit and, at each iteration, the time step is automatically adjusted to ensure numerical stability:

$$\Delta t = C\ \Delta x/(v + c) \tag{4}$$

where C is Courant number (C=1.0 is employed in our simulations), Δx is cell size, v is the computed average

velocity, and c is the computed wave celerity. The time steps typically ranged from 0.01 to 5 s.

The regime can vary between supercritical and subcritical flow. At each time step, flow depth and discharge are computed on a regular grid. Overland flow, sheet flows and flows in rills and gullies are modelled two-dimensionally. Channel flow and street flow are simulated one-dimensionally with channels represented by rectangular or trapezoidal-cross sections using the full-dynamic wave-momentum equation. Channels and streets were identified using georeferenced maps at scales 1:5,000 and 1:25,000 and refined with *ad hoc* field surveys for correct identification of the cross-sections. Channel cross-sections are assigned to a single grid element (or grid elements in a line) containing a channel segment. Overbank flow is modelled when the channel capacity is exceeded, taking into account discharge of the channel to the floodplain or return flow to channel (O'Brien et al. 1993). Infiltration is simulated using the Green-Ampt model, requiring among others, as an input condition, soil permeability, suction and soil moisture (O'Brien 1999).

The mass conservation (balance of inflow, outflow including infiltration, and storage) is satisfied in all simulations with a discrepancy of 1%.

The area selected for the simulation

Qualitatively, under the same general condition (i.e. amount of rain, difference in permeability between the waterproofed areas and soils), syn-eruptive floods will depend on the extension of the waterproofed areas by volcanic ash and the size of the catchment basin considered.

It is reasonable to expect that the volcanic slope will be extensively covered by some decimetres of fine ash during phreatomagmatic activity, whereas dispersion of the ash cover far from the volcano is mainly controlled by the wind regime at different altitudes and by the deposition of pyroclastic density currents at ground level. Erosion can produce local thickening or thinning of the deposits. Thinning is to be expected especially on steep slopes, although these layers may be cohesive and resistant to erosion, especially if dried. All scenarios should therefore be corroborated by a careful collection of field data on the dispersion of these fine-ash layers. However, the geological record is often discontinuous and areas subjected to extensive farming and urbanization make recovery of sections very difficult, especially as regarding late Holocene eruptions. The Vesuvius data mainly refer to areas close to the volcanic vent (e.g. Rosi et al. 1993; Arrighi et al. 2001; Andronico and Cioni 2002) with fewer data available for areas far from the volcano. Some assumptions must therefore be made to integrate the field data. In order to select the scenario for simulating syn-eruptive floods, it is essential that we consider historical, geomorphological and volcanological data, integrated by some assumptions on fine-ash distributions.

Geomorphologically, three different alluvial plains surround Vesuvius: the Acerra-Nola Plain, the Sebeto River Plain and the Sarno River Plain (Fig. 1). Table 1 reports the areal extent of the different catchment areas and the portion of the catchment basin on the slopes of Vesuvius. According to these figures, Vesuvius constitutes a greater percentage of the Sebeto Plain catchment area (~45%) than of the Sarno Plain (~11%) or the Acerra-Nola Plain (~10%). According to the data reported by Cardinali et al. 1998, all three plains were affected in the recent past (1918–1998 period) by flooding, although to a limited extent. Unfortunately, no detailed information is available on these flood events.

Table 1 Catchment extension of the different basins surrounding the Vesuvius volcano. The extension onto the volcanic slope is also reported

Catchment area	Total area (km^2)	Vesuvius catchment contribution (km^2)
Acerra-nola plain	430	44
Sarno plain	540	61
Sebeto plain	97	44

The Acerra-Nola Plain is the most exposed to flood risk. It has no natural outflow to the sea because it is partly closed to the west, near Acerra, by a morphological smoothed ridge that forms a barrier to westward flow, with a minimum at 27 m a.s.l. (Fig. 1). The central part of the Acerra-Nola Plain is also characterised by several hollows (Fig. 1a) that reduce the efficiency of the local outflow (Pareschi et al. 2000b). The areas of the Acerra-Nola Plain that are lower than 27 m a.s.l., account for ~11 km^2 in area. Outlet from the Acerra-Nola Plain is guaranteed by an artificial system of channels developed in the 18th and 19th centuries called the "Regi Lagni".

Geological investigations have shown how the fallout dispersion of Vesuvius varies from E to NE independent of the size of the explosive eruption, and in agreement with the prevailing wind regime in the area (Macedonio et al. 1990; Barberi et al. 1990; Cioni et al. 2003). The only significant exception is the A.D. 79 Plinian eruption (also known as the Pompeii eruption), which had a fallout dispersion toward the south (Sigurdsson et al. 1985) as a result of a wind direction that can occur in late summer (Macedonio et al. 1990). Owing to the described wind regime, the Sebeto Plain has never experienced any large-scale volcanic fallout from Vesuvius, and the Sarno catchment basin has been affected only in its northern part. On the contrary, the Acerra-Nola catchment area has been greatly affected by the deposition of tephra fallout. Dispersion of volcanic material may also be caused by pyroclastic density currents, which are probably an effective long distance means of transport for Plinian eruptions only.

As regards flood hazard zonation, the A.D. 1631 eruption (Rosi et al. 1993; Rolandi et al. 1993a) has been considered as the reference scenario for the "maximum expected event (MEE)" at Vesuvius (Santacroce 1996) and civil protection plans are based on this scenario. Therefore a possible scenario for syn-eruptive flooding starts from this eruption and its effects.

As previously mentioned, historic accounts report that during the eruption of A.D. 1631, wide areas of the Acerra-Nola Plain experienced severe flooding by muddy water

(Rosi et al. 1993, 1996; Nazzaro 1997) fed by the volcano slope but above all by the Apennine slopes (several areas were inundated by more than 2 m of water, for example the Acerra Plain, although it is hard to make a detailed reconstruction of flood depth, Fig. 1b). It has been postulated that the final stage of the A.D. 1631 eruption, with the production of phreatomagmatic fine-grained ash, generated the waterproof effect that reduced infiltration of rainwater, so facilitating overland flow and flooding (Rosi et al. 1996). It is also possible that the volcanic eruption induced atmospheric disturbances which produced anomalous heavy rains. Unfortunately, there are no rain data for the A.D. 1631 eruption, and the analysis of historical rain measurements (which started systematically in the Vesuvian area in the second half of the 19th century) is of no use in establishing a relationship between eruptions and local increase of meteoric precipitation. It is interesting to note, however, that heavy rains were recorded in some rain gauge stations during the eruption of 1906 (Nazzaro 1997).

The A.D. 1631 tephra fallout dispersed mainly toward the east. (Fig. 1). According to statistical analyses on the current prevailing wind regime, an event like that of A.D. 1631 would very likely be dispersed towards the E–NE (Macedonio et al. 1990; Cioni et al. 2003). The dispersion of the fallout shown in Fig. 1 refers to the tephra fall within 10 cm isopach and not to the late phreatomagmatic phases characterised by the production of fine-grained ash deposits. The dispersion of latter deposits is not well constrained far from the volcano due to the lack of measured sections and the measurements available refer to thickness and dispersion of the deposits up to 10–15 km E of the vent of Vesuvius. Their present thickness is disturbed by local erosion and farming activity. Our field investigation on a few scattered points indicates that the ash deposit may be traced up to the Quindici Valley and Sarno Mountains, broadly following the pyroclastic fall.

Overall, historical and stratigraphic data on the A.D. 1631 eruption and statistical analyses of wind distribution (Macedonio et al. 1990) indicate that in the case of renewed volcanic activity with an eruption like MEE, the Clanio Valley and Quindici Valley (Fig. 1a) and catchment areas of the Acerra-Nola Plain could be extensively affected by the volcanic fallout, and presumably by the deposition of fine ashes.

The Acerra-Nola Plain can therefore be considered as potentially the most critical area for flooding in the case of an A.D. 1631-like eruption, and the Acerra-Nola catchment basin as the most disturbed by the effect of the phreatomagmatic ash cover.

The input data

The model requires a number of input data: topographical data, roughness coefficient and soil properties (e.g. suction, hydraulic permeability), in addition to boundary and initial conditions. Topography is specified on a grid of fixed spatial resolution. The topographic data were obtained from a digital elevation model (DEM) derived from spot heights and contour lines (Pareschi et al. 2000a, b). The altimetrical error on spot heights is ± 0.5 m (1σ) and the planimetric error on the contour lines is ± 4 m. For instance, this planimetric error implies a maximum altimetrical error of ~ 0.14 m for slopes $<2^\circ$ (i.e. Acerra-Nola Plain) and ~ 0.85 m for slopes around 25°. Simulations were performed to test the sensitivity of the results to cell sizes, using a uniform roughness coefficient in some sectors of the studied area. With a cell size increasing from 50 to 100 and 200 m, the flooded area (i.e. flood depth >0.5 and >1.0 m) decreased less than 18%. Based on these preliminary simulations, a cell size of 100 m seems the best compromise between acceptable simulation time and need for topographic detail. To reduce the CPU time of the simulation, the study area (about 430 km^2) was divided into four different domains (Fig. 1). The flow exchange between adjacent domains was handled through the insertion of input and output hydrographs at the boundary overlapping cells. These domains are: the Quindici Valley, the Clanio Valley, and the northeastern sector of Somma-Vesuvio and the Acerra-Nola Plain.

Initial conditions are dry channels and an initial degree of soil saturation of 0.32. The soil saturation value is the mean obtained from several soil samples taken during late summer and early autumn (mean 0.32 ± 0.1, range 0.20–0.46, $n=14$). The effect on the different initial soil saturation values was not evaluated.

Ash waterproof effect and soil infiltration

For an eruption similar in magnitude to the A.D. 1631 event, considered here as the reference eruption for flood hazard zonation, the primary assumption introduced in the simulations is the distribution of fine phreatomagmatic ashes inducing a reduction of soil permeability. The assumption made here, based on field data (which is, as already mentioned, fragmentary beyond 10 km from the volcano) is that the fine phreatomagmatic ash covering (emplaced during the final stage of the A.D.1631 event) has the same spatial dispersion as the main tephra deposit, being confined, in our scenario, within the 10-cm-tephra fallout isopach.

Analyses of the permeability of the ash layer covering the coarse tephra of the A.D. 1631 event were performed in the laboratory on undisturbed samples from the volcanic slope and the Apennine slopes. The permeability values range from 1.4×10^{-5} to 5.2×10^{-6} ms^{-1} ($n=17$). Natural soil permeability was measured directly in the field, obtaining mean values of $\sim 10^{-4}$ ms^{-1} ($n=14$). In the simulation, no infiltration was assumed for streets, channels, buildings and impervious topography. In the simulations, ash permeability varied from 10^{-5} to 10^{-6} ms^{-1} and the permeability of natural soils not covered by the ash layer varied between 10^{-4} and 10^{-5} ms^{-1}.

In the illustrated simulations, soil suction was assumed to be 139.7 mm, while ash suction was assumed to be 203.2 mm. Several runs performed with different soil suction values show that the model is not particularly sensitive

to this parameter (Barontini 1999). Variations in suction of $\sim \pm 30\%$ gave variations in depth, extent and velocity of the flow of less than 5%.

Rain data

Since large explosive volcanic eruptions may trigger atmospheric disturbances producing anomalous heavy rains (e.g. Rosi 1996), the simulations of the rainstorms have to take this effect into account. Unfortunately, there are no rainfall data for the A.D. 1631 eruption, and the analyses of historical rain measurements are of no use in establishing a relationship between eruptions and a local increase in meteoric precipitation during post-1631 eruptive activity (Barontini 1999).

In the absence of data on rainfall intensity and its duration during volcanic events, a maximum rain event with a return period frequency of 200 years has been considered. This assumption has a two-fold justification including (1) the 200-year-return period allows assessment of the effects of an unusually heavy rainfall and it should reasonably include the events during an eruption and (2) according to Italian legal requirements, hydraulic structures must be built to resist rain events with this return time (200 years).

Preliminary simulations showed that the concentration time of the catchment area of the Acerra-Nola basin is less than 3 h. The hydrological record analysed was that collected at the rainfall stations located in Lauro (within the Quindici basin) where hourly data have been available since 1957 (the longest time series available for the area with hourly data). For a meteoric event with a duration of 3 h and with a return period of 200 years, the frequency analysis gives, as an extreme value, a rainfall precipitation of 143 mm. The rain distribution used in the simulations was a Gaussian centred histogram homogeneously distributed throughout the area. The constraints on total precipitation (143 mm), duration (3 h) and distribution (Gaussian) led to an event with a maximum peak of rain intensity of 108 mm per 0.5 h.

Roughness

A crucial point in simulations is the roughness coefficient (Manning coefficient). Remote sensing data together with field data and DEM were used to produce thematic maps of land use and land cover in order to assess soil roughness and the related Manning's coefficient. Remote sensing data consisted of Landsat 7 ETM (Enhanced Thematic Mapper), acquired during the summer of 1999 with a spatial resolution of 30 m. Ground truth sites were surveyed by direct inspection or by stereo-pairs aerial photo analysis, and some land-use/cover types were identified (e.g. brush, crops, woodland, urban type). Image-processing techniques were applied to the image data. No atmospheric corrections have been applied to the images because a uniform contribution was assumed. The normalised differentiation vegetation index (NDVI) and tasselled cap (TC) transformations (Niblack 1985; Gupta 1991) were computed to differentiate vegetation cover, soil moisture, soils, rocks and other materials. The principal component transformation (PCT) was also achieved in order to reduce data redundancy and better visualise the different surface types of the landscape. The resulting images (NDVI, TC and PCT) were used to define areas (region of interest, ROI) corresponding to the main land cover types occurring in the region. A supervised classification was then performed on original data by the Spectral Angle Mapper (Jensen 1989). The classification produced a thematic map representing different types of land use and land cover (agricultural, urban, woodland). For each land use type, an appropriate Manning coefficient (O'Brien 1999) was assigned and these values were then used in the simulations (Table 2).

Variations of these Manning coefficients of $\sim \pm 10\%$ produced variations in peak discharge, flow velocity, flow depth and flood extension within $\pm 5\%$. It is difficult to evaluate long-term changes in Manning coefficients (related to long-term land use changes in the next syn-eruptive period). We have performed an additional simulation with an averaged Manning coefficient of 0.05 instead of variable values (0.01–0.1; Table 2). Differences in peak simulated variables are again below 5%.

Table 2 Manning coefficient (*n*-values) used for different land cover and land use

Land use and cover	*n*-values
Industrial factory and working areas	0.013
Densely inhabited place	0.018
Sparsely inhabited place with alternation of small green areas	0.025
Cultivated land	0.04
Grass and shrubs with sparse woods	0.06
Wooded areas	0.07
Dense wood with dense undergrowth	0.1

Results and discussion

The simulations

Three different scenarios were simulated. A first scenario contemplates a case with no occurrence of eruptions and a

Table 3 Summary of the simulations performed with different permeability values for volcanic ash and soil, respectively

Simulation	Ash permeability (ms^{-1})	Soil permeability (ms^{-1})	Direction of ash dispersion
N	–	10^{-4}	–
M1	10^{-5}	10^{-4}	E
M2	10^{-6}	10^{-4}	E
M3	10^{-6}	10^{-5}	E
P1	10^{-5}	10^{-4}	NE
P2	10^{-6}	10^{-4}	NE
P3	10^{-6}	10^{-5}	NE

constant soil permeability of 10^{-4} ms^{-1} (simulation "N"). In the second scenario, a fallout dispersion similar to the A.D. 1631 eruption was simulated and a set of simulations were performed varying soil permeability between 10^{-4} and 10^{-5} ms^{-1} and ash permeability between 10^{-5} and 10^{-6} ms^{-1} (simulations M1, M2 and M3). In the third set of simulations, the impermeable ash area used in simulations M1, M2 and M3 was rotated 30° counterclockwise to match the prevailing wind direction, and the permeability of ash and soil was varied as in the previous scenarios (simulations P1, P2 and P3). To complete the "permeability" scenarios, no infiltration was assumed for streets, channels, buildings and impervious topography. Table 3 summarizes the parameters used in the various simulations.

The range of permeability for the volcanic ash arises from the experimental results. A value in the range 10^{-6}–10^{-5} ms^{-1} can therefore approximate a possible real scenario, while soil permeability of 10^{-4} ms^{-1} is a reasonable assumption for most of the area not covered by ash. The scenario with soil permeability of 10^{-5} ms^{-1} and ash permeability of 10^{-6} ms^{-1} (simulations M3 and P3) is, obviously, a very pessimistic hypothesis. However, this extreme scenario is useful as a boundary for the maximum expected waterproof effect. This can also help us reach a rough estimate of the impact of a very large explosive eruption (e.g. Plinian).

The flooded area

The simulations show how the Acerra-Nola Plain might be affected by severe flooding, in agreement with the historical account (Fig. 1 and 2). For this reason, the next discussion will be focused on this zone, which

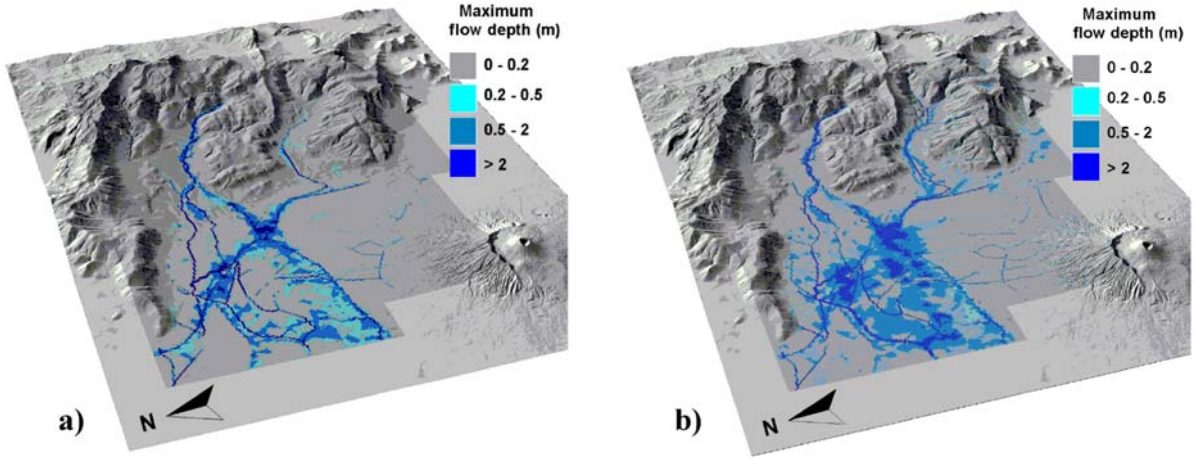

Fig. 2 **a**) Example of flood scenario without an eruption for soil permeability of 10^{-4} ms^{-1} throughout the area and with simulated rains with a return period of 200 years (simulation N). Note that the Acerra-Nola Plain is severely inundated. **b**) Example of flood scenario with occurrence of an eruption like that of A.D. 1631 with ash dispersion towards the east, soil permeability of 10^{-5} ms^{-1} and ash permeability of 10^{-6} ms^{-1}, with simulated rains with a return period of 200 years (simulation M3)

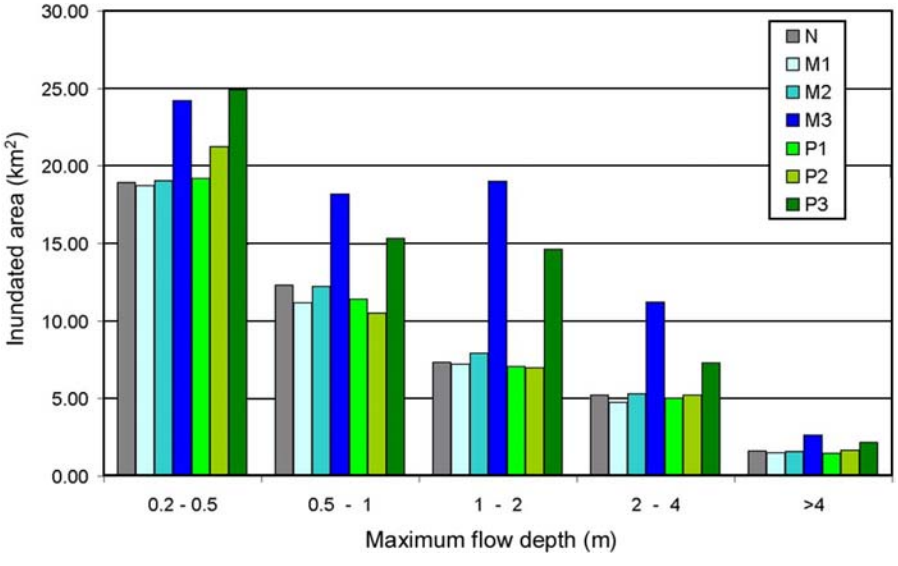

Fig. 3 Distribution of the inundated areas vs. maximum flow depth for different simulations. For permeability values used in the simulations, see Table 3

correspondsy to the NW simulation region defined in Fig. 1a–b. When flow depth is discussed it refers to the maximum flow depth reached during the simulations.

The histograms of Fig. 3 show the distribution of flow depth of the total inundated area in the Acerra-Nola Plain for the different simulated scenarios. As expected, simulations M3 and P3 give the greatest inundated areas, although the total inundated areas with depth >4 m are comparable to the other simulations (Figs. 3 and 4). It is worth noting that the other simulations give comparable results for the total flooded are, although they show some differences in the distribution of flow depth (Fig. 5). There is also an interesting progressive increase of the areas with high flow depth from the M1 simulation to the M3 simulation (Figs. 4 and 5), which is related to the increase of discharge from the Quindici Valley and, to a less extent, from Somma-Vesuvius. In simulation M3, the decrease in infiltration increases the local effect of rainfall stagnation and the greater discharge from the catchment area, which greatly increases the inundated area and the flow depth in the Acerra-Nola Plain. On the contrary, this increase is not particularly evident in the simulation with the NE dispersion of the low

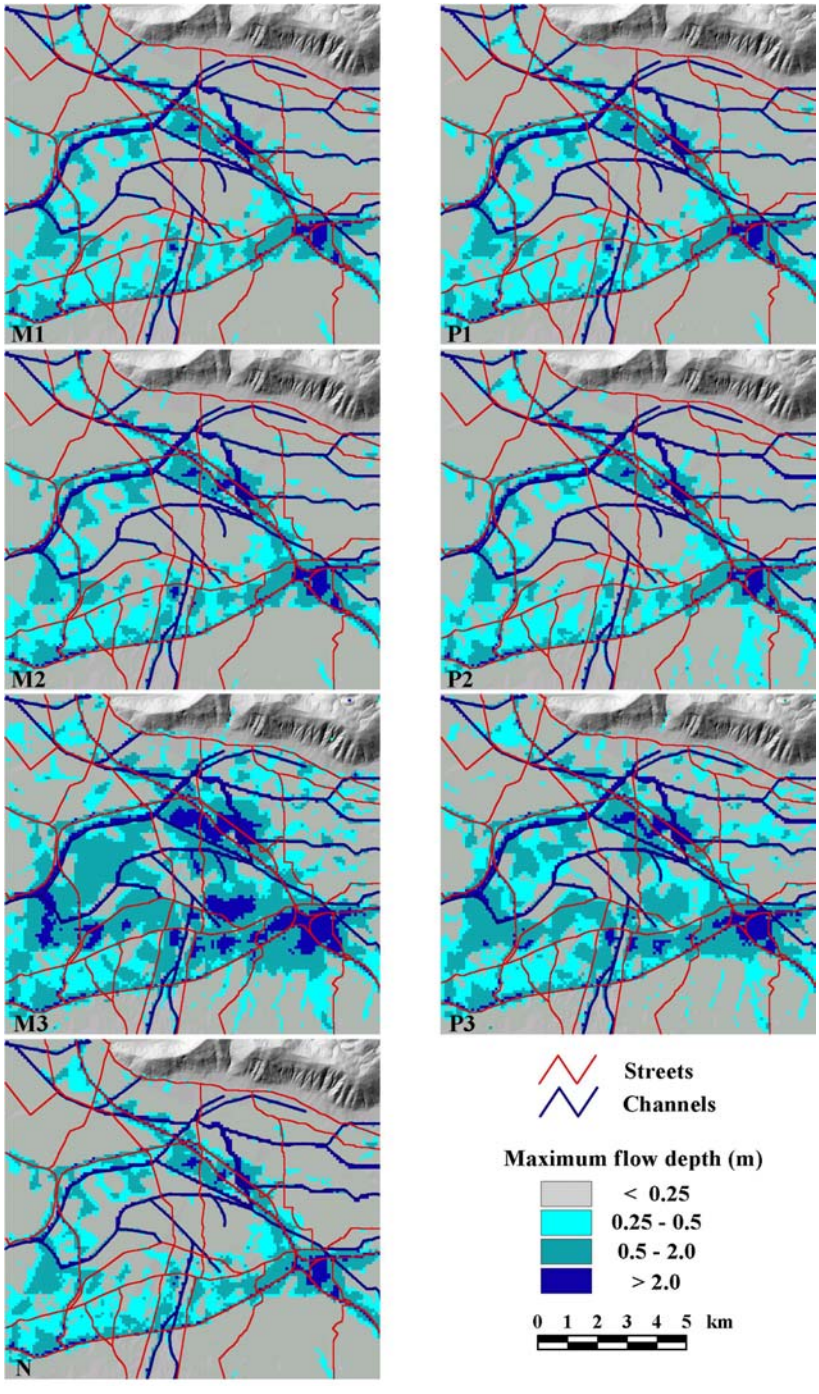

Fig. 4 Maximum flow depth distribution of different simulations for the Acerra-Nola Plain. See Table 3 for the parameter values used

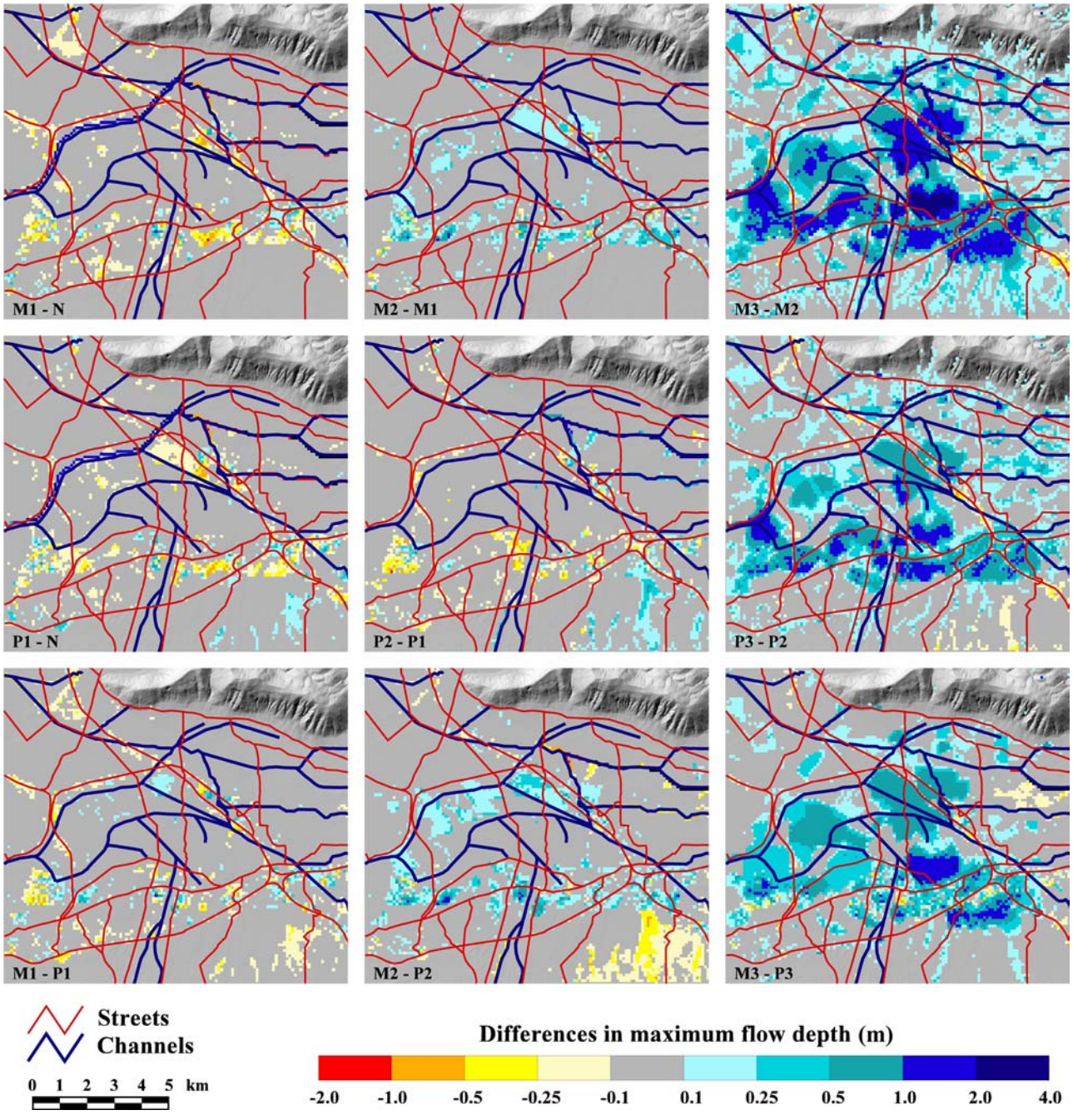

Fig. 5 Selected differences in maximum flow depth for the Acerra-Nola Plain. See Table 3 for the parameter values used

permeability ash. Simulations P1 and P2, in fact, show an increase of flow depth mainly in the area with ash cover, which is a very local effect. The differences between M2-P2 and M3-P3 are good examples of this situation (Fig. 5).

In all the simulations, water is in general concentrated in the low-lying part of the plain, even though the channels and streets seem to exert some control on overbank flooding. Heavy inundations can be observed close to the village of Nola as a consequence of the convergence of water from the Clanio and Quindici valleys.

The analyses of hydrographs (flow depth vs. time) for some selected points help to understand the evolution of the flood and its dynamics (Fig. 6). The selected points correspond to overland areas far from channels or streets. The simulations with eastward ash dispersion usually show the highest flow depth values. This is particularly pronounced in simulation M3. It is also important to emphasise that no particular time lag exists for the different simulations at the same point. Overall, the performed simulations indicate that, under the assumptions made, the Quindici catchment basin controls the extent of flooding into the

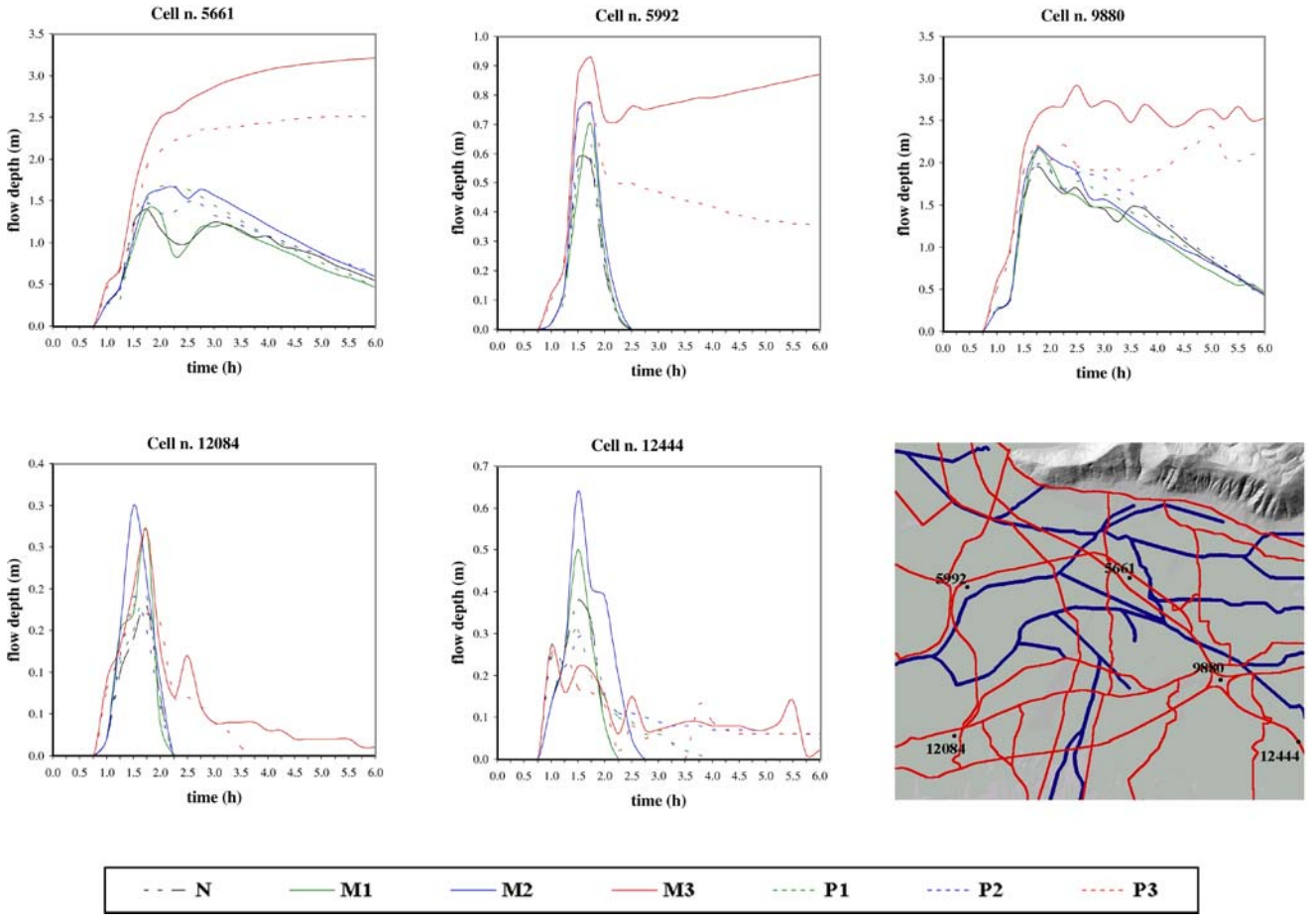

Fig. 6 Hydrographs (flow depth vs. time) for some selected points of different simulations of the Acerra-Nola Plain. See Table 3 for the parameter values used

Acerra-Nola Plain when the effects of an eruption are considered.

To assess the effect of ash waterproofing, an additional simulation was performed assuming a continuous ash layer with a permeability of 10^{-6} ms^{-1} only for the Somma-Vesuvius slope. On the whole, the total discharge towards the Acerra-Nola Plain is small. This demonstrates that the influence of the Somma-Vesuvius slopes is small in comparison to the other basins. This seems to corroborate the hypothesis that floods occurring during the A.D. 1631 eruption were mainly fed by the Apennine drainage network.

From the simulations performed, however, it is possible, methodologically, to define the areas that are at potential risk for flow depths above than a certain value and a flood zonation may be proposed. Three flow heights are chosen to exemplify this approach: 0.5, 1 and 2 m (Fig. 7). Each map of Fig. 7 was divided into three classes: class A, areas that will never attain the given flow depth; class B, areas in which the given flow depth is attained in at least one simulation; class C, the areas in which the given flow depth is attained in all simulations. It is important to keep in mind that this zonation does not take into account the probability of occurrence of the simulated scenarios. According to this approach, the minimum population that could be exposed

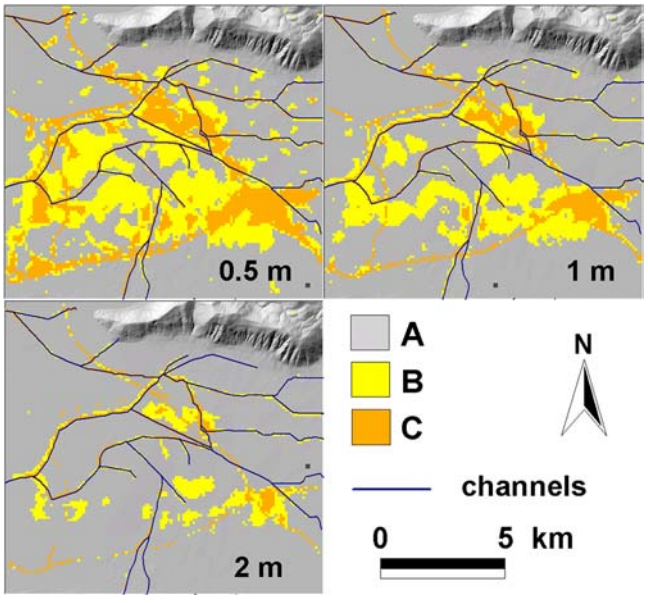

Fig. 7 Possible flood zonation in the Acerra-Nola Plain. Three maximum flow depths are considered: 0.5, 1 and 2 m. Class *A* corresponds to areas where selected flow depth is never attained during the simulations; Class *B* corresponds to areas where selected flow depth is attained at least once; Class *C* corresponds to areas where selected flow depth is attained in all the simulations

to a flood depth >1 m (that is population that may need to be evacuated) is ~40,000 in class B and ~30,000 in class C.

Estimation of total pressures

Water depth is clearly one of the key factors affecting the scale of flood damage together with the duration of flooding. For very shallow flooding, where water does not rise above floor level, damage is unlikely to be significant for most properties (~0–0.5 m). However, predictions of the maximum inundated area should also be accompanied by an estimation of the maximum acting forces, which can help to estimate the potential damage on the exposed values. Such forces also give an estimation of the object size that can be moved forward by the flow. These objects act like missiles, increasing damage and the number of casualties. Moreover, these can also give some indications for the construction of new buildings in order to minimize eventual damage by using flood-resistant materials and utilities, especially for buildings strategically important in the case of renewed volcanic activity. A rough estimation can be performed by taking into account hydrodynamic and hydrostatic pressures. The former are the pressures imposed by the impact of moving water on the upstream side of the structure, drag along the side and eddies, while the latter are the pressures resulting from the static effect of the water at any part of contact with a structure. The total pressures exerted can be simply written as the sum of:

$$P_{\text{total}} = P_{\text{hydrostatic}} + P_{\text{hydrodynamic}} \quad (5)$$

Neglecting eddies and drag effects, the mean total pressure is:

$$P_{\text{total}} = 1/2\rho_{\text{w}} g h + 1/2\rho_{\text{w}} U^2 \quad (6)$$

where ρ_{w} is the water density, g is the gravity acceleration, h is the flow depth and U the mean velocity of the flow. The hydrodynamic pressure is maximal when the flow is perpendicular to structures.

For each point, we calculated the total pressure at two different times: when the hydrostatic pressure was at its maximum and when the dynamic pressure was at its maximum. The maximum value calculated is shown in Fig. 8 for each simulation. The pressure classes used are the same as those developed for the Vesuvian area for pyroclastic flows (Baxter 1998; Zuccaro et al. 1998) to produce a scale of building damage. These values have been supported by static collapse loading tests on different typologies of buildings, windows and doors. Although developed for pyroclastic flows, these values can also be roughly used for floods. According to this damage scale, values above 9 kPa should produce partial to total devastation of a building (Baxter 1998) except for strong aseismic 1–2 storey buildings (structures that collapse over 40 kPa). In several places, the total pressure calculated for the simulated flow may exceed the resistance of buildings (Fig. 8). However, it is important to remember that the total pressure calculated in this way is, in first approximation, an overestimation because the hydrostatic term is progressively balanced if the floodwater enters the buildings. These values should, however, be intended as part of a large-scale study. Indeed, detailed dynamic and hydrostatic forces around individual obstacles can be significantly different from our estimated values.

Concluding remarks

The simulations performed have some severe limitations that should be carefully evaluated in developing them further. Some of the simulations were performed with the intention of estimating these uncertainties. Some uncertainties arise from geological and volcanological assumptions. In particular, the data concerning the dispersion of the phreatomagmatic fine-grained ashes of the A.D. 1631 event are not well constrained. The fact that the simulations performed indicate an underestimation of the dispersion of the ashes is crucial and some scenarios may be too conservative, whereas others may underestimate the effect of the eruption. Moreover, the scenario used for permeability is quite simplified and the effect of rain interception is not considered in detail. Regarding this last point, it is important to remember that the damage to vegetation produced by an eruption is difficult to predict and that data are not available for the study areas. The rainfall scenario is somewhat arbitrary, but in general it could be reasonable in the case of eruption. In spite of these approximations, the simulations of syn-eruptive floods performed in the circumvesuvian area have highlighted some interesting points, which can be useful in the near future to address and improve mitigation plans in case there is renewed eruptive activity of Somma-Vesuvius. Firstly, the simulations have shown how the Acerra-Nola Plain is probably highly vulnerable to inundation with a flood event produced with 200-year-recurrence periods even without the occurrence of an eruption. If the waterproof effect of the volcanic ash layer is considered, our simulations show an even worse hazard, since the maximum depth of the water reached in the Acerra-Nola basin increases. The simulations have also shown the importance of the dispersion of ash. Between the two sets of simulations of the low permeable layer, the more critical case is that of ash dispersion towards the east. In fact, the catchment basin of Quindici is the most important in controlling the extent of flooding in the Acerra-Nola Plain. There are also limits to the topographic information extracted from the DEM. It is well known that the data precision, accuracy and resolution of a DEM are important when defining the final quality and reliability of any predictions of a DEM-based hydrological model (e.g. Kenward et al. 2000; Wolock and Price 1994; Stevens et al. 2002; Thompson et al. 2001; Wang and Yin 1998). Indeed, the quality of a DEM influences the topographical attributes (e.g. slope, aspect, watershed boundary, specific catchment area) and, therefore, the results of hydrological modelling. For instance, with increasing grid size, there is a tendency for hydrologic models to compute an

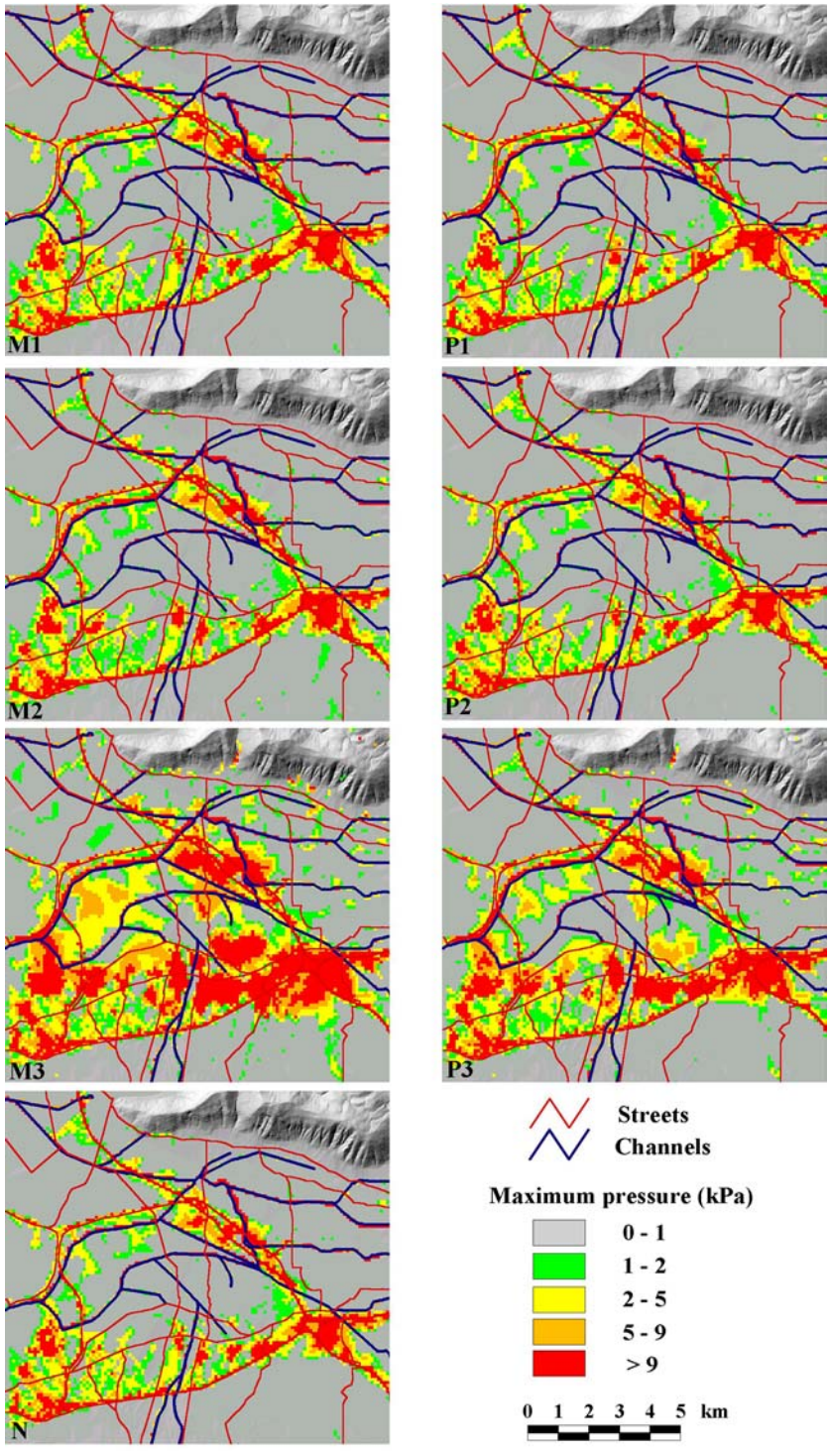

Fig. 8 Maximum total pressure (hydrostatic plus dynamic pressures) obtained from the simulations. See Table 3 for the parameter values used

increase in peak discharge (Zang and Mongomery 1994; Thieken et al. 1999) for a certain catchment. Moreover, Hardy et al. (1999) noted that grid resolution effects were at least as important as a typical calibration parameter. In recent years, the advent of laser altimetry has helped in producing very detailed DEM to deal with flood inundation problems (Horritt 2000; Horritt and Bates 2001). Many examples suggest that a DEM with grid-size resolution of 30–150 m is adequate for reproducing flood inundation (O'Brien et al. 1993; Bates and De Roo 2000), but smaller resolutions are obviously preferable. The use of high resolution topographic information conversely requires a higher resolution of input parameters (e.g. infiltration, roughness data). The uncertainty in the dispersion of ash and the effect of an eruption on meteoric precipitation, and the impossibility of adequately calibrating the results with past events make it wasteful to use a smaller cell-size in our simulation when the model cannot be parameterised with

sufficient accuracy (Hardy et al. 1999). It should, therefore, be emphasised that the results of different simulations are a compromise between model performance and the accuracy of the spatial distribution of the input parameter.

Finally, the effects of the erosion, sediment transport and deposition need some mention. Erosion and deposition are, in general, an important factor in the maintenance of stability of channels, and bridges and the lifetime of a reservoir. Explosive volcanic eruptions typically release a huge quantity of loose material within a few hours or days, thus modifying the bed load and suspended sediment of the channel drastically, and draining the areas affected by primary volcanic deposition (e.g. Rodolfo and Arguden 1991; Montgomery et al. 1999). Because of the existing uncertainties in the model, we have assumed in this phase that the presence of suspended sediment and erosion will produce negligible effects on the final figures, but is clear that, once more data are available, these effects can no longer be neglected and must be modelled, using, for instance, the equation by Hardy et al. (2000).

Acknowledgements This work was supported by the CNR-GNDCI and INGV. We thank S. Cavazza, S. Barontini, V. Caponi, F. Mazzarini, R. Santacroce, M. Rosi, C. Principe and J. O'Brien for the useful suggestions and B.F. Houghton for his constructive revision of an earlier version of the paper. We also thank D. Pyle, D. Pritchard and an anonymous referee for their comments, which greatly improved the quality of the manuscript

References

Andronico D, Cioni R (2002) Contrasting styles of Mount Vesuvius activity in the period between the Avellino and Pompeii Plinian eruptions, and some implications for the assessment of future hazards. Bull Volcanol 64:372–391

Arrighi S, Principe C, Rosi M (2001) Violent Strombolian and sub-Plinian eruptions at Vesuvius during post-1631 activity. Bull Volcanol 63:126–150

Barberi F, Macedonio G, Pareschi MT, Santacroce R (1990) Mapping tephra fallout risk: an example from Vesuvius, Italy. Nature 334:142–144

Barontini S (1999) Studio delle aree alluvionabili nel bacino del Clanio e del Lagno di Quindici in caso di eruzione al Vesuvio. Unpublished Thesis, University of Pisa, Facoltà di Ingegneria, 376 pp

Baxter PJ (1998) Human and structural vulnerability assessment for emergency planning in a future eruption of Vesuvius using volcanic simulation and casualty modelling. EC Project ENV4-CT98-0699 Final Report 51 pp

Bertagnini A, Landi P, Rosi M, Vigliargio A (1998) The Pomici di Base plinian eruption of Somma-Vesuvius. J Volcanol Geotherm Res 83:219–239

Bates PD, De Roo APJ (2000) A simple raster-based model for flood inundation simulation. J Hydrol 236:54–77

Calcaterra D, Parise M, Palma B, Pelella L (1999) The May 5th 1998, landsliding event in Campania (southern Italy): inventory of slope movements in the Quindici area. Yagi N et al. (eds) Proc. Int Symp on Slope Stability Engineering, Balkema, Rotterdam, 1361–1366

Calcaterra D, Parise M, Palma B, Pelella L (2000) Multiple debris-flows in volcaniclastic materials mantling carbonate slopes. Wieczorek GF, Naeser ND (eds) Debris-flow hazard mitigation: mechanics, prediction, and assessment, Balkema, Rotterdam, 99–107

Cardinali M, Cipolla F, Guzzetti F, Lolli O, Pagliacci S, Reichenbach P, Sebastiani C, Tonelli G (1998) Cataologo delle informazioni sulle località italiane colpite da frane e da inondazioni. Publication CNR-GNDCI n. 1799, Perugia

Cerbai I, Principe C (1996) BIBV Bibliography of Historic activity on Italian Volcanoes. CNR-IGGI Internal Report n. 6/96, Perugia

Cioni R, Sbrana A, Vecci R. (1992) Morphological features of juvenile pyroclasts from magmatic to phreatomagmatic deposits of Vesuvius. J Volcanol Geoth Res 51:61–78

Cioni R, Longo A, Macedonio G, Santacroce R, Sbrana A, Sulpizio R, Andronico D (2003) Assessing pyroclastic fall hazard through field data and numerical simulations: the example from Vesuvius. J Geophys Res 108:B2 2063 doi:10.1029/2001JB000642

Gupta RP (1991) Remote sensing geology. Springer, Berlin Heidelberg New York, 356 pp

Hardy RJ, Bates PD, Anderson MG (1999) The importance of spatial resolution in hydraulic models for floodplain environments. J Hydrol 216:124–136

Hardy RJ, Bates PD, Anderson MG (2000) Modelling suspended sediment deposition on fluvial floodplain using a two-dimensional dynamic finite element model. J Hydrol 229:202–218

Horritt MS (2000) Calibration and validation of a 2-dimensional finite element flood flow model using satellite radar imagery. Water Resour Res 36 (11): 3279–3291

Horritt MS, Bates PD (2001) Predicting floodplain inundation: rasted-based modelling versus the finite-element approach. Hydrol Process 15:825–842

Horritt MS, Bates PD (2002) Evaluation of 1D and 2D numerical models for predicting river flood inundation. J Hydrol 268:87–99

Jensen JR (1989) Introductory digital image processing. Prentice-Hall, New Jersey, pp. 379

Kenward T, Lettenmaier DP, Wood EF, Fielding E (2000) Effect of digital elevation model accuracy on hydrologic predictions. Remote Sens Environ 74:432–444

Lirer L, Munno R, Postiglione I, Vinci A, Vitelli L (1997) The A.D. 79 eruption as future explosive scenario in the Vesuvian areas: evaluation of associated risk. Bull Volcanol 59:112–124

Luongo G, Mazzarella A, Palumbo A (1996) On the self-organized critical state of Vesuvio volcano. J Volcanol Geotherm Res 70:67–73

Macedonio G, Pareschi MT, Santacroce R (1990) Renewal of explosive activity at Vesuvius: models for the expected tephra fallout. J. Volcanol Geotherm Res 40:327–342

Major JJ, Pierson TC, Dinehart RL, Costa JE (2000) Sediment yield following severe volcanic disturbance: a two-decade perspective from Mount St. Helens. Geology 28(9):819–82

McKee CO, Johnson RW, Lowestein PL, Riley SJ, Blong RJ, De Saint Ours P, Talai B (1985) Rabaul caldera, Papua New Guinea: volcanic hazard, surveillance, and eruption contingency planning. J Volcanol Geotherm Res 23:195–237

Migale LS, Milone A (1998) Colate rapide di fango nei terreni piroclastici della Campania. Primi dati della ricerca storica. Rass Stor Sal 15(2):253–271

Montgomery DR, Panfil MS, Hayes SK (1999) Channel-bed mobility response to extreme sediment loading at Mount Pinatubo. Geology 27(3):271–274

Nazzaro A (1997) Il Vesuvio. Storia eruttiva e teorie vulcanologiche. Liguori, Napoli 362

Newhall CG, Punongbayan RS eds (1996) Fire and mud: eruption and lahars of Mount Pinatubo, Philippines. Philippine Institute of Volcanology and Seismology, Quezon City, University of Washington Press, Seattle 1126pp

Niblack W (1985) An introduction to digital image processing. Strandberg, Birkeroed, 215 pp

O'Brien JS (1999) Flo-2D users manual version 99.10, 0. Flo Engineering Inc., Palisade, CO

O'Brien JS, Julien PY, Fullerton WT (1993) Two dimensional water flood and mudflow simulation. J Hyd Eng ASCE 119(2):244–259

Pareschi MT (2002) Evaluation of volcanic fallout impact from Vesuvius using GIS. In: Briggs DJ, Forer P, Jarüp L, Stern R (eds) GIS for emergency preparedness and health risk reduction. Kluwer, Dordrecht, pp 101–114

Pareschi MT, Cavarra L, Favalli M, Giannini F, Meriggi A. (2000a) GIS and volcanic risk management. Nat Hazards 21:361–379

Pareschi MT, Santacroce R, Favalli M, Giannini F, Bisson M, Meriggi A, Cavarra L (2000b) Un GIS per il Vesuvio. Felici. 57 pp

Pareschi MT, Favalli M, Giannini F, Sulpizio R, Zanchetta G, Santacroce R (2000c) May 5, 1998, debris flows in circum-vesuvian areas (southern Italy): insights for hazard assessment. Geology 28(7):639–642

Pareschi MT, Santacroce R, Sulpizio R, Zanchetta G (2002) Volcaniclastic debris flows in the Clanio Valley (Campania, Italy): insights for the assessment of hazard potential. Geomorphology 43(3/4):219–231

Rodolfo KS, Arguden AT (1991) Rain-lahar generation and sediment-delivery systems at Mayon volcano, Philippines. In: RV Fisher and GA Smith (eds) Sedimentation in volcanic setting, SEMP Special Publ. 45: 71–87

Rolandi G, Barrella AM, Borrelli A (1993a) The 1631 eruption of Vesuvius. J Volcanol Geotherm Res 58:183–201

Rolandi G, Maraffi S, Petrosino P, Lirer L (1993b) The Ottaviano eruption of Somma-Vesuvius (8000 y.B.P.): a magmatic alternating fall and flow-forming eruption. J Volcanol Geotherm Res 58:43–66

Rolandi G, Mastrolorenzo G, Barrella AM, Borrelli A (1993c) The Avellino plinian eruption of Somma-Vesuvius (3760 y.B.P.): the progressive evolution from magmatic to hydromagmatic style. J Volcanol Geotherm Res 58:67–88

Rosi M (1996) Quantitative reconstruction of recent volcanic activity: a contribution to forecasting future eruptions. In: Scarpa R Tilling RI (eds) Monitoring and mitigation of volcano hazard, Springer Berlin Heidelberg New York, pp. 631–674

Rosi M, Principe C, Vecci R (1993) The 1631 eruption of Vesuvius reconstructed from the review of chronicles and study of deposits. J Volcanol Geotherm Res 58:151–182

Rosi M, Principe C, Cerbai I, Crocetti S (1996). The 1631 eruption. Handbook of the Vesuvius decade Volcano IAVCEI, September 17–22, 1996, Naples, pp 1–12

Santacroce R (1996) Preparing Naples for Vesuvius. Handbook of the Vesuvius decade Volcano IAVCEI,September 17–22 1996, Naples, pp 34–39

Santacroce R (1987) Somma-Vesuvius. CNR Quad Ricerca Sci 114:1–251

Santacroce R, Bertagnini A, Civetta L, Landi P, Sbrana A (1993) Eruptive dynamics and petrogenetic processes in a very shallow magma reservoir: the 1906 eruption of Vesuvius. J Petrol 34(2):383–425

Shimokawa E, Jitousono T (1997) Field survey for debris flow in volcanic area. Armanini A, Michiue M (eds) Recent development on debris flows. Lecture notes in earth sciences, 64 Springer, Berlin Heidelberg New York pp 46–63

Sigurdsson H, Carey S, Cornell W, Pescatore T (1985) The eruption of Vesuvius in 79 A.D. Nat Geogr Res 1:332–387

Stevens NF, Manville V, Heron DW (2002) The sensitivity of a volcanic flow model to digital elevation model accuracy: experiments with digitised map contours and interferometric SAR at Ruapehu and Taranaki volcanoes, New Zealand. J Volcanol Geotherm Res 119:89–105

Thieken AH, Lucke A, Diekkruger B, Richter O (1999) Scaling input data by GIS for hydrological modeling. Hydrol Processes 13:611–630

Thompson JA, Bell JC, Butler CA (2001) Digital elevation model resolution: effects on terrain attribute calculation and quantitative soil-landscape modelling. Geoderma 100:67–89

Todesco M, Neri A, Esposti Ongaro T, Papale P, Macedonio G, Santacroce R, Longo A (2002) Pyroclastic flow hazard assessment at Vesuvius (Italy) by using numerical modeling: I. Large-scale dynamics. Bull Volcanol 64:155–177

Walker GPL (1981) Characteristic of two phreatoplinian ashes, and their water-flushed origin. J Volcanol Goetherm Res 9(4):395–407

Wang X, Yin ZY (1998) A comparison of drainage networks derived from digital elevation models at two scales. J Hydrol 210:221–241

Wolock DM, Price CV (1994) Effects of digital elevation model map scale and data resolution on a topography-based watershed model. Water Resour Res 30:3041–3052

Zanchetta G, Sulpizio R, Pareschi MT, Leoni FM, Santacroce R (2004) Characteristic of May 5–6, 1998 volcaniclastic debris flows in the Sarno areas (Campania, southern Italy): relationships to structural damage and hazard zonation. J Volcanol Geotherm Res 133:377–393

Zhang W, Montgomery DR (1994) Digital elevation model grid size, landscape representation and hydrologic simulations. Water Resour Res 30:1019–1028

Zuccaro G, Baratta A, Petrazzuoli S, Iannello D (1998) Structural vulnerability to possible pyroclastic flows consequent to the eruption of volcano Vesuvius. Final report of the Contribution EC Project ENV4-CT98-0699, Laboratorio di Urbanistica e Pianificazione Teritoriale, University of Naples, Naples, 66 pp